Rapidly Converging Iterative Reconstruction Algorithms in Single-Photon Emission Computed Tomography

Jerold W. Wallis and Tom R. Miller

Mallinckrodt Institute of Radiology, Washington University School of Medicine, St. Louis, Missouri

Iterative reconstruction algorithms with markedly different convergence rates have been proposed in single-photon emission computed tomography (SPECT). Several new iterative reconstruction methods are described in this investigation. Differences between the methods include whether a ramp filter was used during backprojection, the type of backprojection weighting and whether camera and collimator blur were employed in the projection step. Simulated and real cylindrical phantoms with rod inserts were used to compare the properties of convergence and resolution following reconstruction by maximum likelihood (ML), iterative-Chang and the newly proposed reconstruction methods. Resolution was assessed after kernel-sieve regularization to achieve the same signal-to-noise ratio for all methods. Compared with maximum-likelihood reconstruction, methods employing a ramp converged much faster. One such method resulted in images with the same resolution and noise as ML, thus permitting termination of reconstruction at 14 iterations rather than the 1000 iterations required with ML. The major determinants of resolution were found to be use of an accurate model of the gamma camera imaging process in the projection step and inclusion of attenuation weighting and depth-dependent blur in the backprojection step. In summary, a new iterative reconstruction method was developed incorporating attenuation and blur and using a ramp filter that achieved results comparable to maximum-likelihood reconstruction in a fraction of the time.

J Nucl Med 1993; 34:1793–1800

Iterative reconstruction methods have been proposed as a means of improving image quality in single-photon emission computed tomography (SPECT) by reducing noise, enhancing resolution and increasing the accuracy of attenuation compensation. These iterative techniques are not used in clinical practice largely because of the time-consuming nature of many of the algorithms, particularly maximum-likelihood (ML) reconstruction. In this investigation, several new rapidly converging iterative techniques are proposed. Cylindrical resolution phantoms were used to evaluate the results following reconstruction using the new methods, with comparison to the standard techniques of filtered backprojection, the iterative Chang method and maximum-likelihood reconstruction.

Received Jan. 26, 1993; revision accepted May 25, 1993.

For correspondence or reprints contact: Jerold W. Wallis, MD, Mallinckrodt Institute of Radiology, 510 South Kingshighway, St. Louis, MO 63110.

MATERIALS AND METHODS

Reconstruction Algorithms

Many of the iterative algorithms can be viewed as feedback loops in which projections are generated from the current estimate and compared to the measured projections. The difference between the estimated and measured projections, i.e., the "error," is then backprojected and used to update the current estimate. This feedback loop can be seen schematically in Figure 1 and in the iterative reconstruction equations presented in the Appendix.

In more detail:

1. The projection step takes the current estimate and passes it through a simulated gamma camera to produce a series of estimated projections from multiple angles. Reconstruction methods differ in the components of the projection process that are simulated (e.g., attenuation alone or attenuation and collimator blur).
2. The estimated projections are then compared with the measured projections from the same angles obtained during the original gamma camera acquisition. The result of the comparison forms a new "error" projection set. This comparison step can consist of computing the difference or ratio of the pixels in the two data sets, depending on the specific algorithm.
3. The error projections are then backprojected to form an error estimate. Options in the backprojection step include use of a ramp filter and application of weighting factors during backprojection. Weighting factors can be used to more heavily emphasize projection angles closest to a point in the object (potentially improving resolution and noise), to boost counts from the farthest projections (compensating for attenuation), or to spread out the effect of the error corrections by simulation of blur.
4. Some methods then apply a multiplicative correction to the error estimate to partially eliminate attenuation artifacts present after reconstruction with the above steps. The first-order Chang correction (*1*) is an example of a multiplicative correction which compensates for the attenuation during the projection step, albeit imperfectly. If attenuation weighting is explicitly applied during the backprojection step, then a different multiplicative correction would be appropriate. Methods that omit this step eventually achieve attenuation correction through iteration alone.

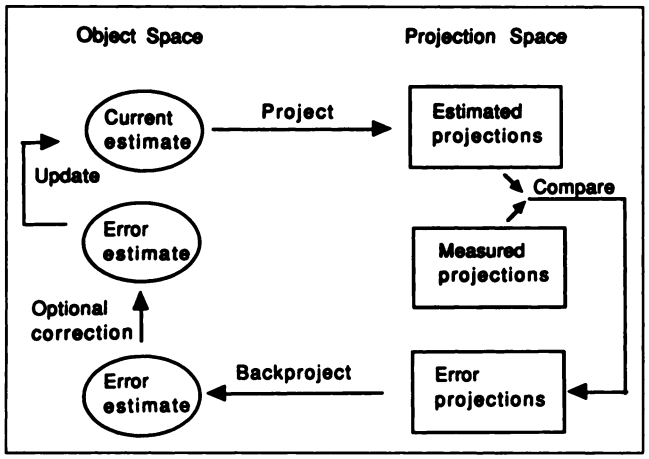

FIGURE 1. Diagram of the feedback loop in iterative reconstruction.

5. The error estimate is then used to update the current estimate. If the comparison consisted of calculating differences, then the update utilizes addition. If the ratios were computed, then the update consists of multiplying the error estimate by the current estimate.

If SPECT reconstruction is viewed as a feedback loop, then conventional filtered backprojection (FBP) can be obtained via a single pass through the loop by starting with an initial estimate of zero (Table 1). This will result in zero for the estimated projections and therefore "error projections" that are identical to the measured projections. Backprojection with a ramp yields the reconstructed image. An optional first-order Chang correction can be applied in the correction step.

The iterative Chang algorithm (*1*) is achieved by multiple passes through this same type of loop (Table 1). The projection step models only attenuation, omitting the gamma camera blur. The multiplicative correction, which compensates for the mean attenuation of each pixel over all angles, is the same as that used in the standard first-order Chang correction.

Maximum-likelihood reconstruction seeks to produce an image that is statistically most likely to yield the observed projections, allowing for attenuation and the Poisson nature of the acquisition process. While maximum-likelihood reconstruction is not intrinsically defined as an iterative method, no single-step method has been found to "invert" the projection process and yield reconstructions directly from the projection data. Iterative methods to approach a maximum-likelihood solution usually employ the expectation-maximization (EM) algorithms developed by Lange et al. (*2*) and Miller et al. (*3*) for SPECT imaging; the former method was implemented in this study. Inspection of these EM-based algorithms show that they can be thought of as feedback loops even though their development was unrelated to this concept. As can be seen in Table 1, maximum-likelihood reconstruction utilizes ratios for comparison and the backprojection step employs weighted backprojection, in which depth-dependent blur is again applied and projections are further attenuated. Updating is then performed by multiplying the reconstructed "ratio" image by the old estimate to give the new estimate. The starting estimate is a constant array, typically with pixel values of unity, rather than the zero-valued array used for the methods employing differences in the comparison step. Unlike the other methods being considered in this investigation, maximum likelihood does not employ a ramp in the backprojection step. The effect of this important omission will be discussed later.

TABLE 1
Iterative SPECT Reconstruction Methods

Method	Project	Compare	Backprojection		Correction
			Weighting ramp		
FBP	(simple)	Difference	none	yes	optional*
It-Chang	Att†	Difference	none	yes	yes
It-Chang-B	Att, Blur‡	Difference	none	yes	yes
It-W1	Att, Blur	Difference	Att	yes	yes
It-W2	Att, Blur	Difference	Att, Blur	yes	yes
ML	Att, Blur	Ratio	Att, Blur	no	no

*If applied, results in first-order Chang correction.
†Att = Attenuation.
‡Blur = Geometric collimator and intrinsic camera blur.

Other reconstruction techniques can be devised that contain the elements of the above methods in different combinations. It is possible to incorporate blur into the projection step in the iterative Chang algorithm (Table 1) with the expectation that this will result in resolution recovery during the iterative process. An algorithm similar to this has been recently proposed by Xu et al. (*4*). Including attenuation-based weighting during the backprojection step serves to give greater weight to projection angles in which the camera is closest, potentially improving resolution and decreasing noise. Weighting based on attenuation alone can be employed (Table 1) or both blur and attenuation can be included in the backprojection weighting as in ML reconstruction (Table 1). The equations for these methods are supplied in the Appendix. All algorithms were constructed so as to allow for nonuniform attenuation with utilization of an attenuation map.

In ML reconstruction, the images become increasingly "noisy" with iterations. As we (*5*) and others (*6,7*) have shown, iterations should not be prematurely terminated. Instead, "regularization" should be applied to control the noise. This phenomenon is also present in the other algorithms evaluated in this work. Here, regularization is achieved by the kernel-sieve method (*6*) in which Gaussian filters are applied to the final reconstruction. The potential effects of other regularization methods are mentioned in the Discussion.

Simulations

A computer-simulated phantom was created consisting of a slice through a cylindrical, four-quadrant resolution phantom. Each quadrant contained square rods alternating between 100% and 50% of peak activity, arranged in a "checkerboard" pattern. This digital phantom is shown in the Results section (Fig. 4). The rod widths varied from 1 cm (2 pixels) to 2.5 cm (5 pixels). Peak activity was set to 75 counts per pixel, chosen to correspond to the maximum count density in a typical hepatic blood pool study. This 64 × 64 noise-free phantom of diameter 25 cm was projected over 360° using 90 angles with simulated uniform attenuation (μ = 0.15/cm); depth-dependent blur was also included, based on measurements from a clinical gamma camera (Multi-SPECT, Siemens Medical Systems, Hoffman Estates, IL). The projections, consisting of 3 million total counts, were then duplicated to form 25 data sets and Poisson noise was added to each projection image to form an ensemble of "noisy" projections. Reconstructions of both the ensemble and selected noise-free data were then performed using the various methods described above.

The contrast between the low and high activity rods in the phantom was measured as an indication of resolution. This approach was viewed as a more accurate measure of resolution than the full-width half-maximum (FWHM) of a line-spread function because of the tendency of some reconstruction algorithms to enhance edges, artifactually narrowing the line-spread function (*7*).

An accurate comparison of algorithms must include measures of both resolution and noise, since one can typically be "traded off" for the other by the choice of filter or regularizer. The signal-to-noise ratio (SNR) for each pixel was measured from the mean and standard deviation of the values at that pixel location in the ensemble of reconstructed images. A mean SNR was then computed for the entire phantom in a manner similar to that employed in our previous work (*5*). Gaussian filters or regularizers were then chosen such that mean SNR was held constant for all numbers of iterations and for all methods. The SNR in the images reconstructed using ML after 50 iterations without regularization was arbitrarily chosen as the level of noise to be achieved after filtering for all methods. After filtering each image in the ensemble with the chosen filter, the images in the ensemble were averaged to produce a mean image. Resolution was then measured from the mean regularized image. Images produced by the iterative-Chang (It-Chang) method were also analyzed following smoothing with a fifth-order Butterworth filter (rather than a Gaussian filter) in order to compare the results with the method widely accepted in clinical practice.

To assess the depth dependence of resolution (*5*) as a function of the method and the number of iterations, resolution was measured separately in the central region of the phantom ($r < 0.5 \times$ radius) and the outer region of the phantom ($r > 0.5 \times$ radius). The contrast values were calculated from the entire width of the rods and represent the mean contrast over rods in the central or outer areas. A two-pixel border around each quadrant was excluded from analysis to avoid inclusion of "spillover" from the adjacent quadrants. The digital phantom used to generate the projections had a contrast value of 0.5. Measured contrast values were plotted as the fraction of this ideal contrast value versus iteration number, with noise held constant.

For illustrative purposes, contrast was also computed for selected regions from nonregularized noise-free reconstructions.

Phantom Data

Projections of a Jaszczak phantom (Data Spectrum Corp., Chapel Hill, NC) filled with 20 mCi of ^{99m}Tc were obtained using a single-head rotating gamma camera (Siemens Orbiter, Siemens Medical Systems, Hoffman Estates, IL) equipped with a high-resolution collimator. Half of the phantom contained only radioactive water and half contained a rod phantom for assessment of resolution. The rod sizes ranged in diameter from 4.8 to 12.7 mm. Data were acquired at 90 angles over 360 degrees into a 128×128 pixel matrix with a pixel size of 3.1×3.1 mm. Several rows of projection data were summed prior to reconstruction to yield a high-count, low-noise study. In the rod portion, this yielded a total of 2,870,000 counts in the 90 projection images. Reconstruction of the central 80×80 pixel region containing the phantom was then performed with each of the methods described above.

Since multiple acquisitions of the rod phantom were not available to permit quantitation of noise in the phantom, reconstructions were also performed of the uniform portion of the phantom, and data from an annulus of the uniform portion of the phantom at a mid-radial position was used to assess noise (*5*). Data from this annular region would be expected to have uniform counts even in the absence of perfect attenuation correction, permitting computation of the signal-to-noise ratio. A regularizer or filter was then chosen to permit evaluation of each method at the same noise level. The signal-to-noise ratio in images produced by 50 iterations of maximum-likelihood reconstruction without regularization was arbitrarily chosen to be the "standard" noise level; images produced by all other methods were regularized to this same signal-to-noise ratio. This level of noise resulted in visually acceptable images, as will be seen below.

Following reconstruction by each method and regularization to equivalent noise levels, images were presented in a blinded manner to five board-certified nuclear medicine physicians, along with a diagram of the "true" rod pattern in the phantom. They were requested to rank the images based on resolution. Ties were permitted, and tied images were given the average of the ranks they would have if they were separable. Results of the blinded rankings were assessed for inter-observer agreement and likelihood of chance occurrence using the Kendall coefficient of concordance (*8*).

RESULTS

Simulations

The graphs in Figure 2 depict contrast in the reconstruction of the noisy data with regularizers applied to achieve identical noise levels. With more iterations, a smoother Gaussian filter had to be applied to achieve a constant noise level. Nearly all methods resulted in reconstructed images with better resolution peripherally than centrally, as described for maximum likelihood reconstruction in our previous work (*5*). (Slight crossing of the inner and outer lines for the 2.0-cm rods in ML and It-W2 at later iteration numbers is due to minimal spillover of counts from adjacent quadrants, despite the 2-pixel border excluded from the region used for calculation.) No method was able to resolve the smallest (1.0 cm) rods at this noise level, and those data were therefore omitted from the graphs.

The graphs for ML and It-W2 are nearly identical, aside from a dramatic difference in convergence rate. The contrast levels achieved by ML after 1000 iterations are comparable to that of It-W2 after 10–12 iterations. The initial contrast values achieved by It-W1 are nearly as good as those with ML, but they decline with successive iterations. Contrast levels achieved by It-Chang-B and It-Chang after Gaussian regularization are inferior to that of ML. Use of a Butterworth filter improved image contrast for It-Chang reconstructions to nearly that of ML, with the exception of the smaller (1.5 cm) central rods.

The resolutions achieved following regularization, shown in Figure 2, depend upon two properties of each algorithm: the ability of the method to deconvolve the camera blurring function and the noise propagation properties of the algorithm. It is useful to examine the former component separately by comparing methods in the absence of noise. Figure 3 depicts the contrast for all methods in the central 1.5-cm rod region of the phantom at successive iterations following reconstruction (without regularization) of noise-free data. All methods which include the model of the camera blur in the projection step yield progressively increasing contrast to approximately the same

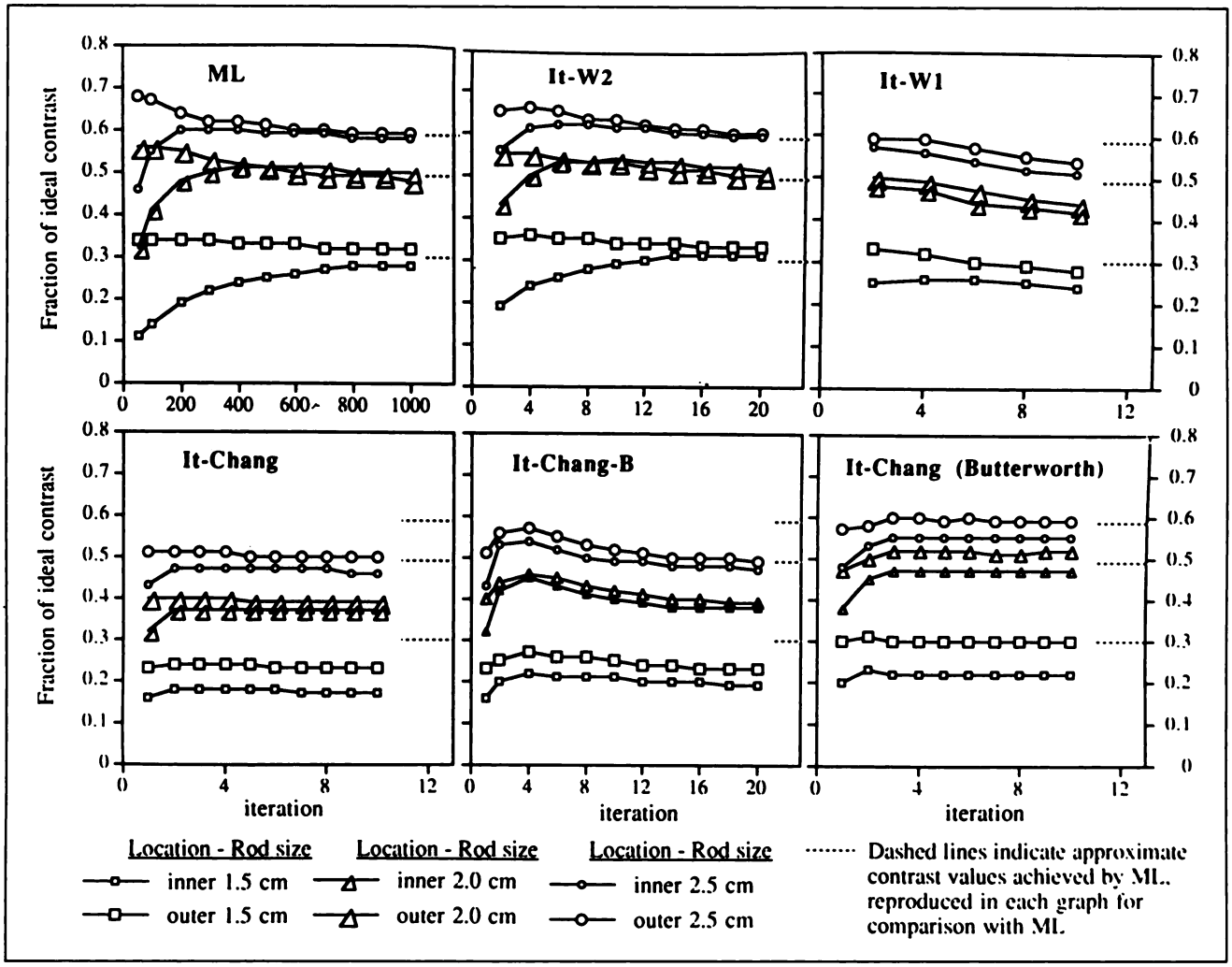

FIGURE 2. Graphs of rod contrast versus iteration number for each of the reconstruction methods. For each of the three different size rods, the smaller symbol represents the central region and the larger symbol corresponds to the outer region. All images were regularized to equivalent noise levels prior to computing contrast. Gaussian filters were used, unless otherwise specified.

value, while little improvement is seen in the method which does not model camera blur (It-Chang). In addition, it can be seen that the algorithms employing a ramp filter converge much more rapidly than those without the ramp filter. For comparison, the It-W2 algorithm is also shown with the ramp filter omitted.

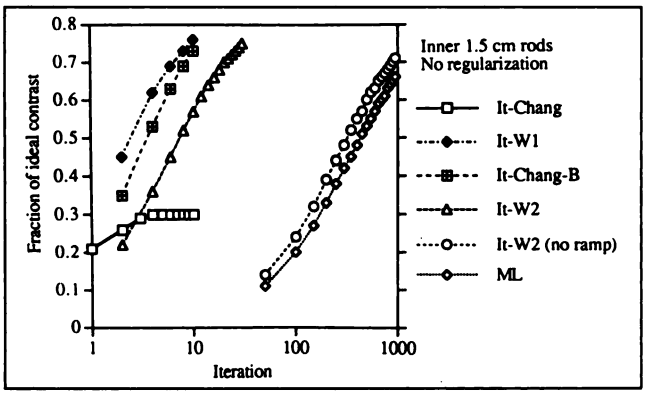

FIGURE 3. Graph of contrast versus iteration for the central 1.5-cm rods, computed from noise-free data without regularization. The difference in convergence rates between algorithms is evident.

Figure 4 contains images corresponding to reconstructions of a single (noisy) instance for each method at a selected number of iterations, as well as an image of the digital phantom used to create the projection data. A minimum of four iterations was chosen for methods that converged rapidly in order to allow time for the attenuation correction to be substantially completed. For the remaining methods, an iteration number was chosen based upon the peak resolution achieved by the method. When there was a difference in convergence rate between the large and small rods, the iteration number was chosen so as to have greatest resolution in the smaller (1.5 cm) quadrant of the phantom.

Phantom Data

The results following reconstruction of the Jaszczak phantom are shown prior to regularization in Figure 5 and after regularization in Figure 6. The methods depicted are ML (1000 iterations), It-W1 (4 iterations), FBP with first-

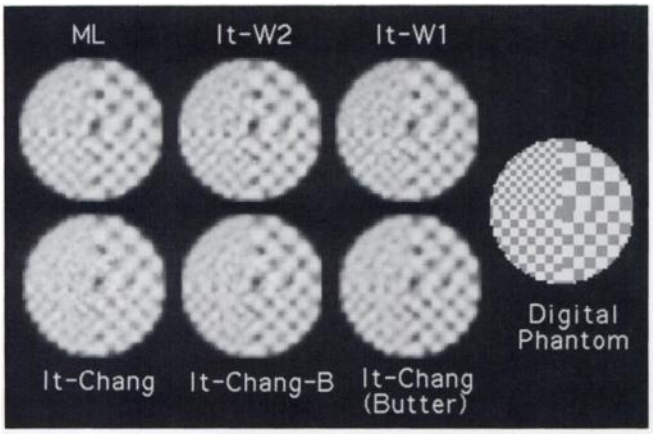

FIGURE 4. Regularized images at the iteration corresponding to maximal resolution for each method, computed from a single (noisy) instance of the simulated phantom. All methods are shown at four iterations with the exception of It-W2 (14 iterations) and ML (1000 iterations). The original image used to generate the projections is also shown.

order Chang, It-W2 (14 iterations), It-Chang-B (4 iterations) and It-Chang (4 iterations). The number of iterations for each method was chosen based upon the previous simulation study. For comparison with conventional reconstruction techniques, the first-order Chang and It-Chang reconstructions are also shown following reconstruction with a fifth-order Butterworth filter, with the filter cutoff chosen to achieve a noise level equivalent to the other methods. The equivalence in noise levels can be confirmed visually by inspection of the upper right sections of the phantom, which contained rods too small to resolve by any of the methods.

The unregularized images (Fig. 5) demonstrate a difference in noise quality between methods employing blur in both the projection and backprojection steps (left), in only the projection step (center) and methods omitting blur

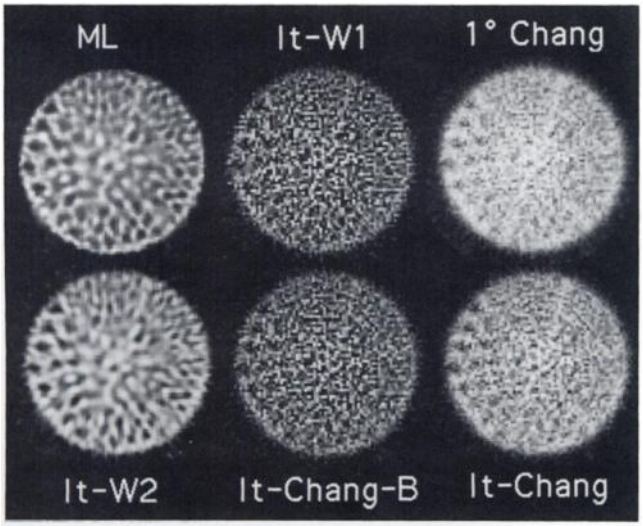

FIGURE 5. Images of the Jaszczak phantom reconstructed by various algorithms, presented without regularization. The methods are: ML (1000 iterations), It-W1 (4 iterations), FBP with first-order Chang, It-W2 (14 iterations), It-Chang-B (4 iterations) and It-Chang (4 iterations).

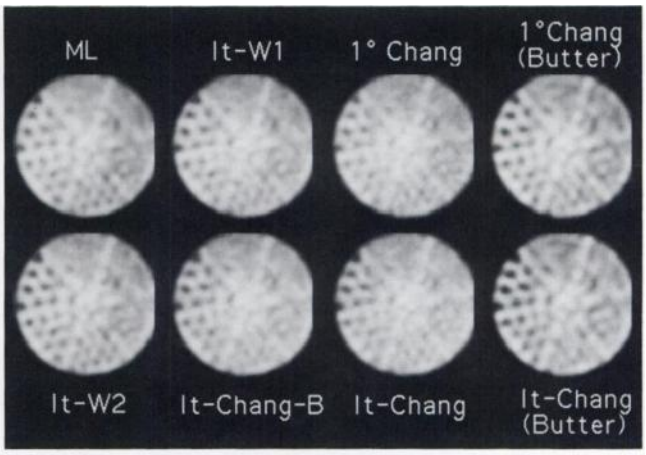

FIGURE 6. Images of the Jaszczak phantom as described in Figure 5, presented after regularization to equivalent noise levels. Images marked "Butter" were smoothed with a fifth-order Butterworth filter; all other images were regularized with a Gaussian filter (slight truncation at the image edge is due to the FIR filter employed). Note the similarity of the ML and It-W2 images in this and the preceding figure, despite the markedly fewer iterations required by It-W2.

(right). The similar appearance between ML and It-W2 is likely due to the fact that they share the same projection and backprojection blur and weighting factors. The "sharpening" effect of incorporating blur into the projection step (center) resulted in increased noise compared to methods without the projection blur (right), thus requiring smoother filters during regularization to achieve comparable noise levels.

Following blinded evaluation of the regularized images in Figure 6, observers selected images produced by It-W2 and ML as having the highest image quality. The methods, arranged from highest ranked to lowest, were as follows (closely ranked methods are listed together, with mean rank in brackets): It-W2 [1.0], ML [2.2]; It-W1 [3.3]; 1°Chang(Butter) [4.1], It-Chang(Butter) [4.9]; It-Chang-B [6.0]; and It-Chang [6.9], 1°Chang [7.6]. This order of image quality was quite consistent between observers (coefficient of concordance 0.88) and was unlikely to have arisen by chance ($p < 0.001$). It-W2 was scored by all observers as superior to the conventional Butterworth-filtered Chang methods.

DISCUSSION

There are two principle conclusions of this work: (1) A ramp-based algorithm with features similar to ML results in convergence speeds that are approximately 80 times faster than ML, yet this faster algorithm produces images that are nearly identical (visually and quantitatively) to those produced by the maximum-likelihood technique; and (2) Inclusion of depth-dependent blur in the projection step and weighting during backprojection result in more optimal use of the available information during iteration, leading to improved resolution.

The first conclusion suggests that the advantages of maximum-likelihood reconstruction may be obtained in clini-

cally practical computation times. A more thorough discussion of our findings is presented below.

What Factors Affect Resolution of the Reconstructed Image?

If the physics of the imaging situation, including gamma-ray attenuation and collimator blur, is modeled correctly, the feedback loop allows the algorithms to recover resolution. With progressive iterations, the feedback loop generates a reconstructed image which, if blurred using the gamma camera response function, yields projections matching the observed projections. Methods that omit the blur during the projection step would not be expected to recover resolution because those algorithms have no knowledge of the blurring function. This difference can be seen most easily by comparison of It-Chang and It-Chang-B in Figure 3, which depicts contrast in the noise-free data. Substantial gain in resolution is seen with iteration for the It-Chang-B method. Minimal improvement seen with the It-Chang method during early iterations is likely associated with attenuation correction.

In the presence of noise, it also becomes critical for the algorithm to have optimal noise properties. If an algorithm amplifies noise with successive iterations, then smoother regularizers need to be applied to maintain a constant noise level. These smoother filters may partially offset the improved resolution achieved by the algorithm. Thus, methods that reach markedly different resolutions in the absence of noise (Fig. 3) may result in only slightly different resolutions when noise is present (Fig. 2). This can be seen by a comparison of It-Chang and It-Chang-B in the two figures.

Introducing weighting in the backprojection step (as is done in ML, It-W1 and It-W2) more heavily weights the "better quality" data from the closer camera angles and will lead to better resolution in the peripheral regions of the image. This effect is most marked in ML and It-W2, which utilize weighting based upon both depth dependent blur and attenuation during backprojection. Including blur in the backprojection weighting slightly slowed convergence but resulted in superior resolution as can be seen by comparing It-W2 and It-W1 (Fig. 2). Including blur while backprojecting also slightly increases the nonuniformity of resolution within the image during early iterations, as observed by us previously for ML reconstructions (*5*). Variable resolution is present to a lesser degree in It-W1, which only employs attenuation weighting. Conventional filtered backprojection also results in mild nonuniformity in the reconstructed image due to the weighting introduced into the projections by the physical attenuation of the emitted gamma rays (*9,10*). Other iterative algorithms using alternate attenuation-based backprojection weighting schemes, such as that proposed by Nowak (*11*), might be expected to yield images similar in quality to It-W1. Tanaka has also proposed a weighted backprojection method (*12*) that could be evaluated using similar techniques.

The type of noise in the unregularized images varies between reconstruction techniques, as is evident from Figure 5. In conventional filtered backprojection, noise is known to be greatest in the higher spatial frequencies, while there is little image content at the high frequencies. This permits use of a "low-pass" Butterworth filter to achieve acceptable noise levels. Use of Butterworth filters in the first-order Chang and It-Chang reconstructions resulted in substantially improved resolution compared to that achieved by Gaussian regularization; this can be seen both visually and quantitatively by comparison of It-Chang to It-Chang (Butterworth) in Figures 2, 4 and 6. In the simulations, use of a Butterworth filter also improved resolution for the It-W2 method (data not shown); however, further investigation is needed to decide whether the Butterworth filter is appropriate, given the different noise content.

Which Algorithm Yielded the Best Resolution?

The simulation study employing rod phantoms suggested that It-W2 and ML had the highest resolution, followed by It-W1 and It-Chang (Butterworth). The measurement of camera resolution using bar phantoms (for planar gamma cameras) and rod phantoms (for tomographic imaging) is well established, and is especially appropriate in this situation where point-spread-functions may be misleading due to potential edge artifact. Typically, examination of the smallest resolvable bar or rod yields the best indication of image resolution. The gain in resolution when comparing It-W2 to It-Chang (Butterworth) is most evident in the simulations when examining the contrast in the central 1.5-cm rods (Fig. 2). The contrast achieved by It-W2 was comparable to the contrast present after filtering the original digital phantom with a 12-mm Gaussian filter, while that of It-Chang (Butterworth) was comparable to that after filtering the digital phantom with a 14-mm Gaussian filter. This gain in resolution was also apparent to all of the observers during the blinded evaluation of the real phantom data. The slight (apparent) superiority of It-W2 over ML in the observer experiment likely reflects the fact that 1000 iterations of ML may not yet have converged as much as 14 iterations of It-W2. This is also suggested in the simulations by the graphs in Figure 2.

A receiver-operating characteristic (ROC) study involving patient images will be needed to determine if ML and It-W2 have superior diagnostic performance compared to other methods.

Why Are Some Algorithms Slower to Converge Than Others?

The key factor affecting the speed of convergence of the iterative algorithms appears to be use of the ramp filter in the backprojection of the error term. The slowest algorithm (ML) lacked a ramp filter during the backprojection step. Omitting the ramp filter will produce a blurred image after backprojection, as observed in the original backprojection reconstruction employed by Kuhl (*13*). Thus, in these iterative methods, the ramp acts to "sharpen" or "focus" the error into the correct region of the reconstructed slice

leading to faster convergence. Without the ramp, the feedback loop eventually compensates for the 1/R blurring introduced by the backprojection operation, but many iterations are required. This can be seen in Figure 3 which shows that omission of the ramp filter from It-W2 results in slowing of the convergence rate by a factor of 50. Omission of blur from the backprojection step also speeds convergence to a minor degree (see It-W1 versus It-W2 in Fig. 3), though at some loss in resolution (Fig. 2).

Other Considerations

A frequently mentioned advantage of maximum-likelihood reconstruction is the non-negativity of the reconstructions (*14,15*). The other iterative methods evaluated here can lead to negative pixel values because of the presence of the ramp filter. To avoid this possibility, negative values were set to zero at each iteration; omission of this non-negativity constraint in simulations resulted in increased image noise.

Here, kernel sieve regularization was employed; other forms of regularization (e.g., use of Gibb's priors (*16,17,18*) or Good's roughness penalty (*19,20*)) may yield improved results for all the iterative reconstruction methods. However, their use would have hindered the type of noise analysis employed in this investigation since the regularization could not be performed interactively after reconstruction to achieve comparable noise levels. It is unlikely that these other forms of regularization (applied in the same way to all methods) would significantly change the relative ordering of the various algorithms, although further work will be required to confirm this conjecture.

Although the simulations employed in this study did not include scatter, this fact should not bias the results in favor of any particular algorithm, since none modeled scatter in the reconstruction process. Additionally, the nonsimulated Jaszczak phantom data containing significant scatter yielded reconstructed images supporting the conclusions generated from the computer simulations. Addition of scatter correction to the reconstruction algorithms would likely improve the results with real data without altering the fundamental conclusions of this work.

Several reconstruction methods were omitted from this analysis (e.g., ART, SIRT); a complete survey of all existing and possible methods is beyond the scope of this investigation. To the extent that these other methods can be thought of as feedback loops, the basic conclusions of this work may well apply.

CONCLUSION

This comparison of iterative reconstruction algorithms in SPECT suggests that camera and collimator blur and attenuation should be employed in both the projection and backprojection steps to achieve optimal results. A new algorithm employing a ramp filter as part of each iteration is proposed which yields images equivalent in resolution and noise to maximum likelihood, while dramatically increasing the convergence rate of the algorithm. Use of a very fast iterative algorithm, such as conventional iterative-Chang, or a slowly converging algorithm, such as maximum likelihood, will lead to inferior images or slow reconstruction compared to the new method.

APPENDIX

The equations for the reconstruction algorithms employ the terminology of McCarthy and Miller (*21*). The equations below assume a two-dimensional image with reconstruction of a single slice. The slice to be reconstructed consists of points $x = (x, y) \in \Re^2$, where $\lambda(x)$ is the source distribution. The detector rotates in a circular orbit about the center of the slice. At each angle θ, events are measured at points u on the detector, and the number of detected events at each point is $M(u, \theta)$.

If there were perfect collimation, for each angle θ the point x would project onto the detector at a unique point $P_\theta(x)$. Due to blur, the actual detected events are spread out over multiple points u, where the position error e is given by $e = u - P_\theta(x)$. The error in position, which represents the camera blur, conforms to a distribution $p(e|x, \theta)$ that is approximately Gaussian in shape.

The recorded counts $M(u, \theta)$ are also a function of attenuation $\beta(x, u, \theta)$. The attenuation term represents the probability of measurement of a photon traveling from point x towards detector point u at angle θ, where

$$\beta(x, u, \theta) = \exp\left(-\int_{L(x,u)} \mu(l)\, dl\right). \qquad \text{Eq. A1}$$

The line $L(x, u)$ corresponds to the path from x to point u on the detector, and $\mu(l)$ is the linear attenuation coefficient at point l along the path. The overall detection probability $\bar{\beta}(x)$ for a collimated photon emanating from x may be obtained by computing the mean of $\beta(x, u, \theta)$ for points $u = P_\theta(x)$ over the angles θ.

Thus, a discrete model of the projection step, incorporating both attenuation and blur is:

$$\hat{\mu}^{(k)}(u, \theta) = \sum_x p(e|x, \theta)\beta(x, u, \theta)\hat{\lambda}^{(k)}(x), \qquad \text{Eq. A2}$$

where $\hat{\lambda}^{(k)}(x)$ is the estimated source distribution at iteration k, and $\hat{\mu}^{(k)}(u, \theta)$ is the estimated projection at the k^{th} iteration. Methods that omit blur employ a modified delta function instead of $p(e|x, \theta)$ to provide linear interpolation:

$$\begin{aligned} \delta(e|x, \theta) &= 0 \quad \text{if } e| > |1, \\ &= 1 \quad \text{if } |e| = 0, \\ &= 1 - |e| \quad \text{if } 0 < |e| < 1, \end{aligned}$$

where e is in units of pixels.

The iterative ML algorithm utilizes Equation A2 for projection, and the complete algorithm for the estimated source distribution at iteration $k + 1$, $\hat{\lambda}^{(k+1)}(x)$, is given by

$$\hat{\lambda}^{(k+1)}(x) = \hat{\lambda}^{(k)}(x) \frac{1}{\bar{\beta}(x)} \sum_\theta \sum_u p(e|x, \theta)\beta(x, u, \theta) \cdot \left[\frac{M(u, \theta)}{\hat{\mu}^{(k)}(u, \theta)}\right], \qquad \text{Eq. A3}$$

TABLE A1
Equation Components of the Iterative Methods

Method	C(x)	Blur	Att
It-Chang*	$1/\bar{\beta}(x)$	$\delta(\theta\|x, \theta)$	1
It-Chang-B	$1/\bar{\beta}(x)$	$\delta(\theta\|x, \theta)$	1
It-W1	$(1/\bar{\beta}(x))^2$	$\delta(\theta\|x, \theta)$	$\beta(x, u, \theta)$
It-W2	$(1/\bar{\beta}(x))^2$	$p(\theta\|x, \theta)$	$\beta(x, u, \theta)$

*In projection step (Eq. A2) $p(\theta|x, u, \theta)$ is replaced by $\delta(\theta|x, \theta)$

or, in English,

$$\hat{\lambda}^{(k+1)}(x) = \hat{\lambda}^{(k)}(x) \frac{1}{Mean\_Att} \sum_{\theta} \sum_{u} Blur \cdot Att \cdot \left[\frac{Measured\_projection}{Estimated\_projection}\right], \quad \text{Eq. A4}$$

where the summation ($\Sigma\Sigma$) performs the backprojection operation.

In this form, it is easy to see that the ratio of the measured and estimated projection values are being backprojected (with blur and attenuation) to update the current estimate. The term $1/Mean\_Att$ serves to "compensate" for the attenuation introduced by the attenuation in the backprojection step; it is not commonly considered to be a multiplicative correction, although it is in some ways analogous to $C(x)$, described below.

The general form for the iterative methods utilizing differences (rather than ratios) for the comparison step is:

$$\hat{\lambda}^{(k+1)} = \hat{\lambda}^{(k)}(x) + K \cdot C(x) \cdot \left(\sum_{\theta} \sum_{u} Blur \cdot Att \cdot R \otimes [Measured\_proj.-Estimated\ proj.] \right), \quad \text{Eq. A5}$$

where $R\otimes$ represents one-dimensional convolution with a ramp filter prior to backprojection, $C(x)$ indicates a (spatially varying) multiplicative correction and K represents a scale factor employed to compensate for scaling introduced by our implementation of the backprojection operation and ramp convolution. K was determined after the first iteration by comparison of the total counts in a projection of $\hat{\lambda}^{(1)}$ with the total counts in the measured projections. Optionally, a "relaxation factor" could be incorporated into K to help prevent divergence of the algorithm, although that was not done in this implementation. Differences rather than ratios were chosen for the comparison step of It-W1 and It-W2 in order to accommodate negative values that might be generated by ramp filtering of the error projections. Following each iteration, in order to introduce a nonnegativity constraint, all negative values in the estimate were set to zero.

Using this general form, the other algorithms that were evaluated were constructed as shown in Table 1A. They all include the ramp and employ Equation 2A for the projection step to produce the estimated projections.

All methods were implemented on a DECstation 5000/200 workstation (Digital Equipment Corp., Maynard, MA) using the acceleration techniques described by us previously (*22*).

REFERENCES

1. Chang LT. A method for attenuation correction in radionuclide computed tomography. *IEEE Trans Nucl Sci* 1978;26:638–643.
2. Lange K, Carson R. EM reconstruction algorithms for emission and transmission tomography. *J Comp Assist Tomogr* 1984;8:306–316.
3. Miller MI, Snyder DL, Miller TR. Maximum-likelihood reconstruction for single-photon emission computed tomography. *IEEE Trans Nucl Sci* 1985; NS-32:769–778.
4. Xu XL, Liow JS, Strother SC. An iterative linear algorithm based on filtered backprojection for image reconstruction [Abstract]. *J Nucl Med* 1992;33: 871–872.
5. Miller TR, Wallis JW. Clinically important characteristics of maximum-likelihood reconstruction. *J Nucl Med* 1992;33:1678–1684.
6. Snyder DL, Miller MI. The use of sieves to stabilize images produced with the EM algorithm for emission tomography. *IEEE Trans Nucl Sci* 1985;32: 3864–3872.
7. Snyder DL, Miller MI, Thomas LJ Jr, Politte DG. Noise and edge artifacts in maximum-likelihood reconstruction for emission tomography. *IEEE Trans Med Imaging* 1987;6:228–237.
8. Wilkinson L, Hill M, Vang E. *Systat: statistics*. Evanston, IL: Systat, Inc.; 1992.
9. Manglos S, Jaszczak R, Floyd C, Hahn L, Greer K, Coleman R. Nonisotropic attenuation in SPECT: phantom tests of quantitative effects and compensation techniques. *J Nucl Med* 1987;28:1584–1591.
10. Knesaurek K, King M, Glick S, Penney B. Investigation of causes of geometric distortion in 180° and 360° angular sampling in SPECT. *J Nucl Med* 1989;30:1666–1675.
11. Nowak DJ, Eisner RL, Fajman WA. Distance-weighted backprojection: a SPECT reconstruction technique. *Radiology* 1986;159:531–536.
12. Tanaka E. Quantitative image reconstruction with weighted backprojection for single photon emission computed tomography. *J Comput Asst Tomogr* 1983;7:692–700.
13. Kuhl D, Edwards R. Image separation radioisotope scanning. *Radiology* 1963;80:653–61.
14. Shepp LA, Vardi Y. Maximum likelihood reconstruction for emission tomography. *IEEE Trans Med Imaging* 1982;1:113–122.
15. Chornoboy ES, Chen CJ, Miller MI, Miller TR, Snyder DL. An evaluation of maximum likelihood reconstruction for SPECT. *IEEE Trans Med Imaging* 1090;9:99–110.
16. Hebert T, Leahy R. A generalized EM algorithm for 3-D Bayesian reconstruction from Poisson data using Gibbs priors. *IEEE Trans Med Imaging* 1989;8:194–202.
17. Lalush DS, Tsui BMW. Simulation evaluation of Gibbs prior distributions for use in maximum A Posteriori SPECT reconstructions. *IEEE Trans Med Imaging* 1992;11:267–275.
18. Lange K. Convergence of EM image reconstruction algorithms with Gibbs smoothing. *IEEE Trans Med Imaging* 1990;9:439–446.
19. Miller MI, Roysam B. Bayesian image reconstruction for emission tomography incorporating Good's roughness prior on massively parallel processors. *Proc Natl Academy Sci* 1991;88:3223–3227.
20. Butler CS, Miller MI. Maximum a posteriori estimation for SPECT using regularization techniques on massively-parallel computers. *IEEE Trans Med Imaging* 1993;12:84–89.
21. McCarthy AW, Miller MI. Maximum-likelihood SPECT in clinical computation times using mesh-connected parallel computers. *IEEE Trans Nucl Sci* 1991;10:426–436.
22. Miller TR, Wallis JW. Fast maximum-likelihood reconstruction. *J Nucl Med* 1992;33:1710–1711.